CrossMark

# Photoinduced one-pot synthesis of hydroxamic acids from aldehydes through in-situ generated silver nanoclusters

Yasser M. A. Mohamed[1] · Yasser A. Attia[2] · Eirik Johansson Solum[3]

## Abstract

Hydroxamic acids have attracted significant attention due to their widespread use in applied chemistry. In this report, a modified Angeli–Rimini method has been achieved via the visible light-mediated catalytic transformation of a variety of heterocyclic, aromatic and aliphatic aldehydes **1a–j** to their corresponding hydroxamic acids **2a–j** in 81–93% yield. The unique ability of vitamin $K_3$ as a photoredox catalyst to expedite the development of completely new reaction mechanisms and to enable the construction of challenging carbon–nitrogen bonds has been investigated. It is shown for the first time that the vitamin $K_3$ and aldehyde are largely responsible for rapid in situ reduction of $Ag^+$ ions to catalytic photoluminescent Ag nanoclusters that possess a bandgap energy of 2.87 eV and are less than 2 nm in size. A mechanism for this reaction has been proposed and is supported by UV–Vis, TEM, ESI/MS, FT-IR, $^1$H NMR and $^{13}$C NMR analyses. The investigated method utilizes readily available reagents and produces the hydroxamic acids in high yields without the formation of side products, making it simple, practical and cost-effective.

✉ Yasser M. A. Mohamed
   y.m.a.mohamed@outlook.com

✉ Yasser A. Attia
   yasserniles@niles.edu.eg

[1]  Photochemistry Department, National Research Center, Dokki, Giza 12622, Egypt

[2]  National Institute of Laser Enhanced Sciences, Cairo University, Giza 12613, Egypt

[3]  Faculty of Health Sciences, NORD University, 7800 Namsos, Norway

⚫ Springer

## Introduction

Over the past few decades, the Angeli–Rimini reaction has enabled the synthesis of hydroxamic acids from aldehydes and *N*-hydroxybenzene sulfonamide in the presence of strong base [1]. However, this method has several drawbacks, including the formation of a by-product which is difficult to remove from the desired product, and low yields. To date, various methods for the preparation of hydroxamic acids have been developed, including the reaction of nitroarenes with aldehydes in the presence of Mn-oxide as a catalyst [2], the reaction of nitrosoarenes with aldehydes catalysed by *N*-heterocyclic carbenes [3], the oxidative amidation of alcohols [4], hydroacylation of aldehydes using dialkyl azodicarboxylates in the presence of phenylglyoxylic acid [5], and the reaction of activated carboxylic acids, acyl halides or esters with O-protected, N,O-protected [6–9] and unprotected hydroxylamines [10]. However, these synthetic approaches often require drastic conditions, long reaction times and the use of expensive reagents. Hence, due to the importance of hydroxamic acids as therapeutic agents [11, 12] and strong metal ion-chelators [13, 14], the development of new procedures for the synthesis of hydroxamic acids is imperative. Specifically, reaction efficiency and product isolation can be facilitated by the minimization of stoichiometric chemical waste. The exploration of new concepts in the area of nanocluster photocatalysis provides opportunities to develop novel green syntheses of valuable fine chemicals [15–19]. Recently, nanoclusters have been extensively examined as active catalysts for several reactions [20–22], including the oxidation of CO to $CO_2$ [23], the NO–CO reaction [24], $H_2$ production by way of photocatalytic water splitting [25], and the formation of formaldehyde (HCHO) and methanol ($CH_3OH$) from CO and $H_2$ [26]. Silver nanoclusters have evolved to be used in sophisticated strategies in catalysis due to their interesting luminescence properties [27, 28]. To date, many synthetic methods have been developed to obtain colloidal silver nanoclusters such as direct chemical reduction and photo- or thermally-induced transformations [25, 29]. The preparation of water-soluble Ag clusters has also been demonstrated [30, 31]. Additionally, the synthesis of Ag clusters using templated assemblies such as DNA [32–34], polypeptides [35, 36], and proteins [37, 38] has been reported. Herein, the Ag nanoclusters have generally been produced from the reduction of $Ag^+$ ions under photoredox catalysis conditions. One attractive aspect of this protocol is the utilization of Ag nanoclusters as intermediates in the visible light-driven catalytic conversion of a set of aldehydes to their corresponding hydroxamic acids through a nucleophilic addition reaction.

## Experimental

### Materials and methods

All chemicals were obtained from Sigma-Aldrich and used without further purification. All melting points (mp) are uncorrected. Thin-layer chromatography (TLC) was performed using silica gel plates 60 GF254, cellulose plates

(20 × 20 cm). The infrared spectra were recorded as a thin film on a PerkinElmer FT-IR spectrometer. The nuclear magnetic resonance (NMR) spectra were obtained on a Bruker Avance DPX (300 MHz for $^1$H and 75 MHz for and $^{13}$C, respectively). The chemical shift data are reported in parts per million (ppm) downfield from tetramethylsilane. DMSO-$d_6$ was as partial deuterated-NMR solvent. UV–Vis spectra were recorded on a Hewlett-Packard 8452A diode-array spectrophotometer. Photoluminescence spectra were measured on a FP-8200 spectrofluorometer (Jasco). X-ray diffraction (XRD) measurements were performed using a Philips PW1710 X-ray diffractometer using Cu Ka radiation ($k = 1.54186$ Å). The XRD patterns were recorded from 20° to 70° $^2$H, with a step size of 0.020° $^2$H and collecting 10 s per step. Transmission electron microscopy (TEM) micrographs of the colloidal particles were measured using a JEOL JEM-2100 of 200 kV with a magnification range of 1000× to 50,000×. The TEM samples were prepared and placed on a copper grid by mixing one dilute drop of prepared aqueous particles dispersed in 5 mL acetone to produce a slightly turbid solution that was allowed to dry thoroughly. High-resolution mass (ESI/MS) spectra were recorded on an Agilent 6230 Series accurate-mass time-of-flight (TOF) LC/MS.

## General procedure for nicotine hydroxamic acid (2a) using the classical Angeli–Rimini reaction

To a solution of N-hydroxybenzene sulfonamide (0.17 g, 1 mmol) in MeOH (2 mL), MeONa (0.11 g, 2 mmol) was added. Pyridine-3-carboxaldehyde (**1a**) (0.11 g, 1 mmol) was subsequently added and the reaction mixture was stirred at room temperature for 24 h. The reaction was monitored by TLC. After completion of the reaction, the mixture was concentrated and EtOAc (30 mL) was added. The organic layer was collected, dried over anhydrous MgSO$_4$ and then the solvent was evaporated under reduced pressure using a rotatory evaporator. The obtained residue was purified by a short plug of silica gel using (hexane:EtOAc, 1:1) to afford N-hydroxynicotinamide (**2a**) in 55% yield.

## General procedure for the photosynthesis of hydroxamic acids 2a–j

To an aqueous solution of AgNO$_3$ (1.7 mg, 0.01 mmol, 1 mol%) in water (6 mL), vitamin K$_3$ (2.6 mg, 0.015 mmol, 1.5 mol%) dissolved in ethanol (2 mL) was added, and then an appropriate aldehyde (1 mmol) dissolved in THF (2 mL) was added to the reaction mixture followed by the addition of NH$_2$OH·HCl (69 mg, 1 mmol) and Et$_3$N (0.14 mL, 1 mmol). The final solvent ratio (H$_2$O:EtOH:THF) was (3:1:1). The mixture was stirred at room temperature for 30 min under visible light irradiation using a halogen lamp (HALOPAR 20 75 W 230 V 30-GU10; Osram, Italy). The reaction was monitored by TLC. After completion of the reaction, EtOAc (30 mL) was added. The aqueous layer was collected and concentrated under reduced pressure at 25 °C to obtain pure sample containing Ag nanoparticles that was characterized by UV–Vis and TEM analyses. The organic phase was collected, dried over anhydrous MgSO$_4$ and filtered. The solvent was evaporated under vacuum using a rotatory evaporator and then the residue was

purified by a short plug of silica gel using (Hexane:EtOAc, 1:1) to obtain hydroxamic acids **2a–j** in 81–92% yield.

## Characterization data for compounds 2a–j

### N-hydroxynicotinamide (2a)

White solid (93%); mp 136–137 °C [Literature [39] mp 135 °C]; $^1$H NMR (300 MHz, DMSO-$d_6$): δ (ppm) 10.16 (br, s, 1H), 9.44 (br, s, 1H), 8.62 (d, $J$ = 4.2 Hz, 1H), 8.09 (d, $J$ = 7.8 Hz, 1H), 7.76–7.74 (m, 1H), 7.36–7.32 (m, 1H); $^{13}$C NMR (75 MHz, DMSO-$d_6$): δ (ppm) 168.2, 152.5, 147.6, 136.8, 129.3, 126.0; HRMS (ESI) m/z [M + H]$^+$ calcd for $C_6H_7N_2O_2$ 139.0508, found 139.0572.

### N-hydroxypicolinamide (2b)

Yellow solid (91%); mp 154–155 °C; $^1$H NMR (300 MHz, DMSO-$d_6$): δ (ppm) 10.32 (br, s, 1H), 9.36 (br, s, 1H), 8.78 (d, $J$ = 8.4 Hz, 2H), 7.64 (d, $J$ = 8.4 Hz, 2H); $^{13}$C NMR (75 MHz, DMSO-$d_6$): δ (ppm) 167.2, 152.5, 143.4, 122.5; HRMS (ESI) m/z [M + H]$^+$ calcd for $C_6H_7N_2O_2$ 139.0508, found 139.0556.

### N-hydroxyfuran-2-carboxamide (2c)

White solid (87%); mp 126–127 °C; $^1$H NMR (300 MHz, DMSO-$d_6$): δ (ppm) 10.35 (br, s, 1H), 8.72 (br, s, 1H), 6.95-7.16 (m, 2H), 7.79 (d, $J$ = 6.5 Hz, 1H), 8.80 (br, s, 1H); $^{13}$C NMR (75 MHz, DMSO-$d_6$): δ (ppm) 164.5, 147.9, 144.7, 119.7, 112.3; HRMS (ESI) m/z [M + H]$^+$ calcd for $C_5H_5NO_3$: 128.0348, found 128.0352.

### N-hydroxythiophene-2-carboxamide (2d)

Off-white solid (89%); mp 123–124 °C [Literature [1] mp 122–123 °C]; $^1$H NMR (300 MHz, DMSO-$d_6$): δ (ppm) 6.92–7.04 (m, 2H), 7.16 (d, $J$ = 6.2 Hz, 1H), 9.42 (br, s, 1H), 10.81 (br, s, 1H); $^{13}$C NMR (75 MHz, DMSO-$d_6$): δ (ppm) 160.8, 136.7, 132.0, 127.6, 127.2; HRMS (ESI) m/z [M + H]$^+$ calcd for $C_5H_5NO_2S$: 144.0119, found 144.0213.

### N-hydroxybenzamide (2e)

Off-white solid (85%); mp 125–126 °C [Literature [40] mp 127 °C]; $^1$H NMR (300 MHz, DMSO-$d_6$): δ (ppm) 10.97 (br, s, 1H), 0.8.75 (br, s, 1H), 7.69–7.62 (m, 2H), 7.51-7.48 (m, 3H); $^{13}$C NMR (75 MHz, DMSO-$d_6$): δ (ppm) 165.3, 132.9, 132.1, 129.4, 127.1; HRMS (ESI) m/z [M + H]$^+$ calcd for $C_7H_8NO_2$: 138.0555, found 138.0527.

### N,2-dihydroxybenzamide (2f)

Brown solid (83%); mp 176–177 °C; ^{1}H NMR (300 MHz, DMSO-$d_6$): $\delta$ (ppm) 12.15 (br, s, 1H), 11.76 (br, s, 1H), 9.81 (br, s, 1H), 7.64 (d, $J$ = 7.8 Hz, 1H), 7.51 (t, $J$ = 7.8 Hz, 1H), 6.99-6.94 (m, 2H); ^{13}C NMR (75 MHz, DMSO-$d_6$): $\delta$ (ppm) 168.5, 160.6, 136.3, 129.4, 122.1, 119.4, 117.1; HRMS (ESI) m/z [M + H]$^+$ calcd for $C_7H_8NO_3$: 154.0504, found 154.0516.

### N-hydroxy-3-phenylpropanamide (2g)

White solid (86%); mp 71–72 °C [Literature [41] mp 69–72 °C]; ^{1}H NMR (300 MHz, DMSO-$d_6$): $\delta$ (ppm) 9.11 (br, s, 1H), 8.76 (br, s, 1H), 7.28–7.16 (m, 5H), 2.82 (t, $J$ = 7.5, 2H), 2.39 (t, $J$ = 7.5, 2H); ^{13}C NMR (75 MHz, DMSO-$d_6$): $\delta$ (ppm) 169.8, 140.9, 128.8, 128.5, 126.6, 35.3, 31.6; HRMS (ESI) m/z [M + H]$^+$ calcd for $C_9H_{13}NO_2$: 166.0868, found 166.0862.

### N-hydroxypentanamide (2h)

White solid (92%); mp 54–55 °C [Literature [42] mp 53–54 °C]; ^{1}H NMR (300 MHz, DMSO-$d_6$): $\delta$ (ppm) 10.02 (br, s, 1H), 9.36 (br, s, 1H), 2.11 (t, $J$ = 7.1 Hz, 2H), 1.57 (m, 2H), 1.30 (m, 2H), 0.88 (t, $J$ = 7.1 Hz, 3H); ^{13}C NMR (75 MHz, DMSO-$d_6$): $\delta$ (ppm): $\delta$ (ppm) 171.2, 32.6, 28.0, 22.6, 14.1. HRMS (ESI) m/z [M + H]$^+$ calcd for $C_5H_{12}NO_2$: 118.0868, found 118.0853.

### N-hydroxy-2-methylpentanamide (2i)

White solid (81%); mp 80–81 °C, ^{1}H NMR (300 MHz, DMSO-$d_6$): $\delta$ (ppm) 10.41 (br, s, 1H), 8.65 (br, s, 1H), 2.11–1.84 (m, 1H), 1.53–1.29 (m, 2H), 1.22–1.06 (m, 2H), 0.88 (d, $J$ = 6.9 Hz, 3H), 0.77 (t, $J$ = 7.1 Hz, 3H); ^{13}C NMR (75 MHz, DMSO-$d_6$): $\delta$ (ppm) 172.2, 36.8, 35.2, 20.1, 18.4, 14.0; The NMR data are in agreement with the literature [23]; HRMS (ESI) m/z [M + H]$^+$ calcd for $C_6H_{14}NO_2$: 132.1052, found 132.01057.

### N-hydroxyicosanamide (2j)

White solid (90%); mp 102–103 °C; ^{1}H NMR (300 MHz, DMSO-$d_6$): $\delta$ 10.23 (br, s, 1H), 9.74 (br, s, 1H), 2.39 (td, $J$ = 7.4, 1.9 Hz, 2H), 1.64–1.56 (m, 2H), 1.34–1.22 (m, 32H), 0.82 (t, $J$ = 6.9 Hz, 3H); ^{13}C NMR (75 MHz, DMSO-$d_6$): $\delta$ 172.3, 44.3, 32.3, 30.2 (8CH$_2$), 30.1, 30.0, 29.9, 29.8, 29.7, 29.6, 23.1, 22.5, 14.5; HRMS Calcd for $C_{20}H_{42}NO$ [M + 1]$^+$ 328.3216, found 328.3214.

## Results and discussion

In this protocol, it was demonstrated that vitamin $K_3$ was a potential photoredox catalyst which played an important role as an effective electron carrier and electron transfer agent [43–45] in the reduction of $Ag^+$ ions to Ag nanoclusters due to the reactivity of the quinone moiety upon excitation under visible light. In an initial series of experiments, it was observed that the reaction between vitamin $K_3$ and pyridine-3-carboxaldehyde (**1a**) and hydroxylamine under visible light irradiation resulted in the production of pyridine-3-hydroxamic acid (**2a**) through the in situ formation of Ag nanoclusters as active catalysts (Scheme 1).

The UV–Vis analysis of an aqueous solution provided evidence for the formation of Ag nanoclusters, which showed no absorption peaks in the UV–visible region [25], while the photoluminescence measurement showed a peak with maximum intensity at $\lambda = 432$ nm at an excitation wavelength of 310 nm, constituting the first indication of the formation of Ag clusters [25, 27] (Fig. 1a). The value of the bandgap can be estimated using the emission peak energy (432 nm, i.e. 2.87 eV). Although the TEM technique is not the best method for characterizing the size of the metal clusters because of cluster fusion [25], the HRTEM image in Fig. 1b showed fine distribution of Ag clusters with sizes below 2 nm.

A possible reaction mechanism for the synthesis of hydroxamic acids is illustrated in Scheme 2.

In Scheme 2, pyridine-3-carboxaldehyde (**1a**) was converted into nicotine hydroxamic acid (**2a**) via the formation of an acyl cation, an intermediate which is known to be reactive towards nucleophiles. Thus, when the $Ag_n$-NOH group attacked this cation, hydroxamic acid **2a** was obtained. This proposed mechanism is supported by FT-IR data. After 5 min of reaction progress, the IR spectrum provided evidence for the formation of Ag nanoclusters via ionic interaction and complexation with the present scaffolds which have multiple functional groups (OH, CHO and NOH) that allow strong interaction with $Ag^+$ ions (Fig. 2).

As shown in the FT-IR spectrum, the appearance of a broad band at 4218 cm$^{-1}$ is due to the presence of (NOH) groups attached to Ag clusters in the form $Ag_n$(NOH). The OH groups of vitamin $K_3H_2$ (see Scheme 2) appeared at 3688 and 3620 cm$^{-1}$ which confirmed the conversion of vitamin $K_3$ to its isomeric form; vitamin $K_3H_2$ under the action of light. The C=O of aldehyde **1a** appeared at 1717 cm$^{-1}$. Characteristics band for the N–O stretch appeared at 1586, 1478 cm$^{-1}$ and the C–O stretch band appeared at 1220 cm$^{-1}$. In addition, the reaction was monitored by an off-line ESI/MS spectrometer. Characteristic peaks were observed for nicotine
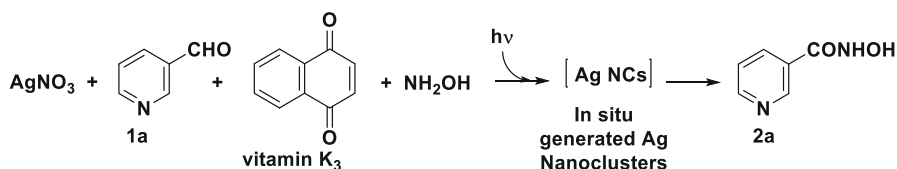


**Scheme 1** A model reaction: in-situ formation of Ag nanoclusters and their catalytic activity towards the synthesis of hydroxamic acid **2a** from aldehyde **1a**
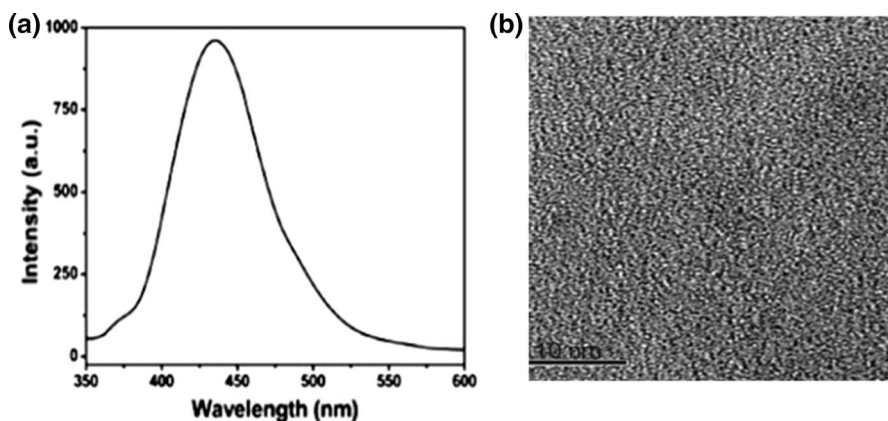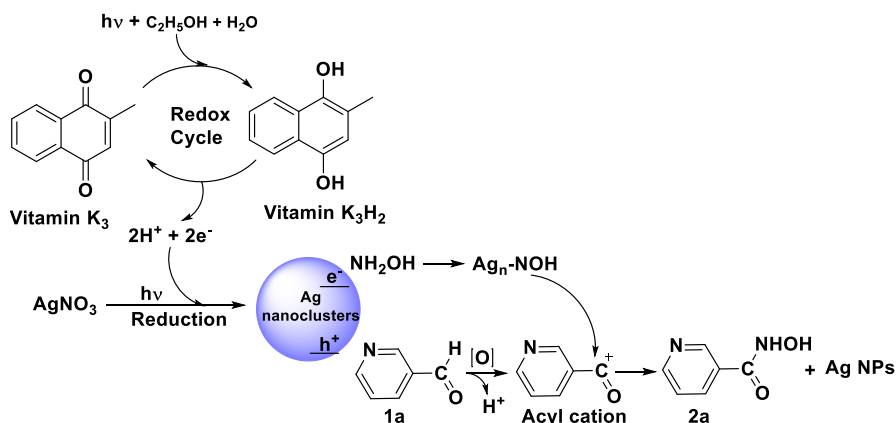
Fig. 1 **a** Photoluminescence spectrum of the formed Ag nanoclusters from the aqueous solution of the reaction after 5 min; **b** TEM image of Ag nanoclusters



Scheme 2  Proposed reaction mechanism for the modified Angeli–Rimini procedure

hydroxamic acid (**2a**) (m/z $[M + 1]^+ = 139.0572$), unreacted pyridine-3-carbox-aldehyde (**1a**) (m/z $[M + 1]^+ = 108.0446$), and vitamin K$_3$ (m/z $[M + 1]^+ = 173.0979$) in addition to other characteristic peaks at m/z = 525.9054, 555.7309 and 663.8046, respectively, indicating the formation of Ag$_2$ and Ag$_3$ nanoclusters with mixed ligands (Table 1).

Complete conversion of pyridine-3-carboxaldehyde to nicotine hydroxamic acid was observed after 30 min which was confirmed by $^1$H and $^{13}$C NMR spectral measurements of the isolated organic substrate. The $^1$H NMR spectrum showed two peaks at $\delta = 10.16$ and 9.44 ppm, respectively characteristic for NH and OH groups present in hydroxamic acid. In addition, $^{13}$C NMR showed the characteristic peak of (CONHOH) at $\delta = 168.2$ ppm without the appearance of a significant peak for the (CHO) group (see Fig. 3a–d).
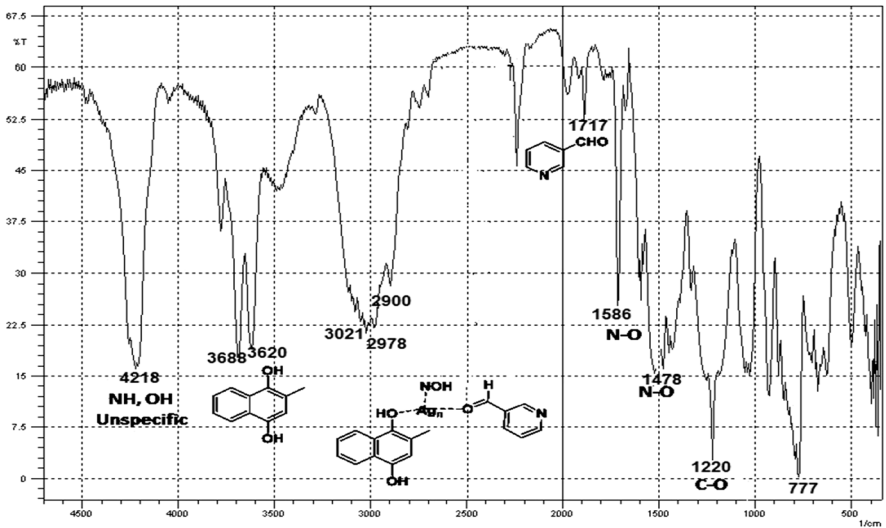
**Fig. 2** FT-IR spectrum of the supernatant of the reaction mixture

**Table 1** Molecular formula of identified peaks

| m/z | Expected molecular formula |
|---|---|
| 525.9054 | $(C_{11}H_8O_2)(C_6H_5ON)Ag_2$-(HNO) |
| 555.7309 | $(C_{11}H_8O_2)(C_6H_5ON)Ag_2$-(HNO)$_2$ |
| 663.8046 | $C_{11}H_8O_2)(C_6H_5ON)Ag_3$-(HNO) |
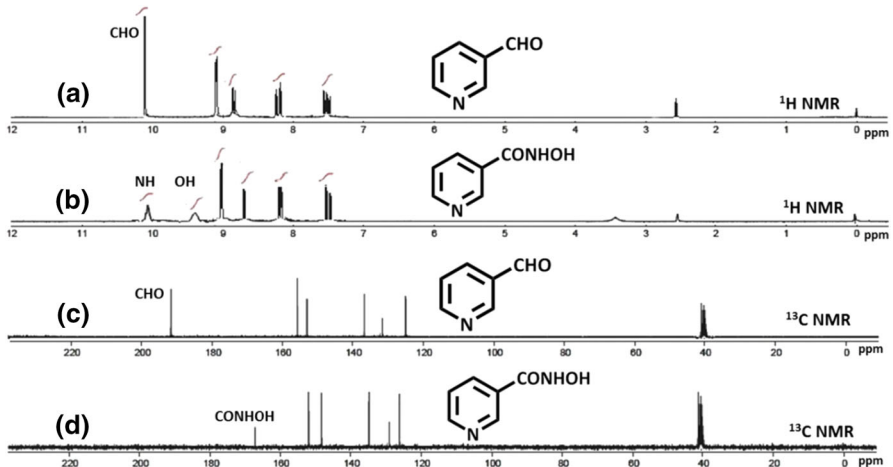


**Fig. 3** **a** $^1$H NMR spectrum of pyridine-3-carboxaldehyde; **b** $^1$H NMR spectrum of the isolated organic substrate indicating the formation of nicotine hydroxamic acid; **c** $^{13}$C NMR spectrum of pyridine-3-carboxaldehyde; **d** $^{13}$C NMR spectrum of hydroxamic acid

**Scheme 3** Pyridine-3-carboxaldehyde as model substrate for the Angeli–Rimini reaction

For completeness, we examined the reaction (Scheme 3) under various conditions (Table 2).

It was observed that the reaction between the aldehyde and hydroxylamine in the absence of catalyst did not proceed (Table 2, entry 1). In addition, in the presence of AgNO$_3$ (Table 2, entry 2), in the dark or under visible light, respectively, the aldehyde was recovered. Also, when we employed the catalytic system (AgNO$_3$/vitamin K$_3$) in the dark, the aldehyde was recovered (Table 2, entry 3). However, interestingly, the use of AgNO$_3$/vitamin K$_3$ under visible light (Table 2, entry 4) delivered the hydroxamic acid **2a** in excellent yield (93%), which indicates that light is necessary for the reaction. Finally, a classical Angeli–Rimini reaction was performed and gave nicotine hydroxamic acid in 55% yield after 24 h (Table 2, entry 5). From the above results, a modified methodology for the Angeli–Rimini protocol was designed by the reaction of AgNO$_3$, aldehyde and hydroxylamine in the presence of vitamin K$_3$ as a photoredox catalyst due to its ability to transfer

**Table 2** Screening of different reaction conditions used in the synthesis of nicotine hydroxamic acid from pyridine-3-carboxaldehyde

| Entry | Additives | Reaction conditions | Yield % |
|---|---|---|---|
| 1 | Without catalyst[a] | In dark or under visible light | n.d. |
| 2 | AgNO$_3$[b] | In dark or under visible light | n.d. |
| 3 | AgNO$_3$/vitamin K$_3$[c] | In dark | n.d. |
| 4 | AgNO$_3$/vitamin K$_3$[d] | Under visible light | 93% |
| 5 | N-hydroxybenzene sulfonamide/MeONa[e] | Room temperature | 55% |

*n.d.* not detected

[a]Reaction conditions: pyridine-3-carboxaldehyde (**1a**) (1 equivalent), NH$_2$OH·HCl (1 equivalent), Et$_3$N (1 equivalent) in H$_2$O:EtOH:THF (3:1:1) stirred at room temperature under visible light for 24 h
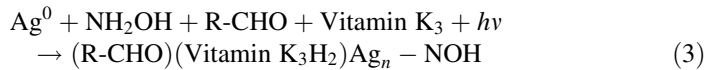
[b]Reaction conditions: pyridine-3-carboxaldehyde **3a** (1 equivalent), NH$_2$OH·HCl (1 equivalent), Et$_3$N (1 equivalent), AgNO$_3$ (1 mol%) in H$_2$O:EtOH:THF (3:3:1) stirred in the dark or under visible light for 24 h

[c]Reaction conditions: pyridine-3-carboxaldehyde (**1a**) (1 equivalent), NH$_2$OH/HCl (1 equivalent), Et$_3$N (1 equivalent), AgNO$_3$ (1 mol%), vitamin K$_3$ (1.5 mol%) in H$_2$O:EtOH:THF (3:1:1) stirred in the dark for 48 h

[d]Reaction conditions: pyridine-3-carboxaldehyde (**1a**) (1 equivalent), NH$_2$OH·HCl (1 equivalent), Et$_3$N (1 equivalent), AgNO$_3$ (1 mol%), vitamin K$_3$ (1.5 mol%) in H$_2$O:EtOH:THF (3:1:1) stirred under visible light for 30 min

[e]Conditions for the classical Angeli–Rimini reaction: pyridine-3-carboxaldehyde (**1a**) (1 equivalent), MeONa (2 equivalent), N-hydroxybenzene sulfonamide (1 equivalent) in MeOH. The reaction was stirred under ambient conditions at room temperature for 24 h

electrons via excitation under visible light [43–45]. Herein, it was demonstrated that vitamin $K_3$ induced electron transfer through oxidative-reductive modes in aqueous solution upon excitation by using visible light. Silver ions were then reduced to form silver nanoparticles as shown below in Eqs. 1 and 2.

$$Vitamin\ K_3 + hv + C_2H_5OH/H_2O + 2e^- \leftrightarrow Vitamin\ K_3H_2 \tag{1}$$

$$AgNO_3 + e^- \rightarrow Ag^0 + NO_3^- \tag{2}$$
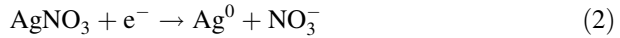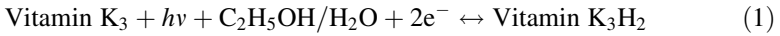
The Ag cluster was formed via the reaction of Ag nanoparticles with aldehyde, hydroxylamine and vitamin $K_3$ (Eq. 3), as evidenced by ESI/MS and IR data.

$$\begin{aligned} Ag^0 + NH_2OH + R\text{-}CHO + Vitamin\ K_3 + hv \\ \rightarrow (R\text{-}CHO)(Vitamin\ K_3H_2)Ag_n - NOH \end{aligned} \tag{3}$$

By way of a sequential pathway, the $Ag_n$-NOH adduct reacted with the aldehyde to afford hydroxamic acid and Ag nanoparticles (Eq. 4).

$$(R\text{-}CHO)(Vitamin\ K_3H_2)Ag_n\ \text{-}\ NOH + R\text{-}CHO + hv \rightarrow R\text{-}CONHOH + Ag^0 \tag{4}$$
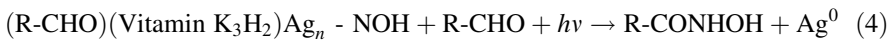
It was shown that this transformation was facilitated by the powerful catalytic activity of in situ formed Ag nanoclusters that possess powerful semiconducting properties with a bandgap of $\sim 3$ eV [27, 46]. At the end of the reaction, the presence of a surface plasmon resonance absorption peak at 403 nm revealed the formation of Ag NPs (Fig. 4a). In addition, a representative TEM image showed that the solution consists of Ag NPs with an average size of about $4.6 \pm 1.81$ nm due to aggregation of clusters to larger nanoparticles (Fig. 4b) which was considered as new evidence for the proposed mechanism. Also, XRD patterns corresponding to the (111), (200) and (220) planes of the formed Ag NPs (Fig. 4c) were observed at $2\theta$ angles of $38.25°$, $44.32°$ and $64.51°$, respectively [47].

Finally, the methodology was successfully applied to the synthesis of a series of hydroxamic acid derivatives. A set of photocatalytic reactions were performed between an array of aldehydes, including pyridine-4-carboxaldehyde **1b**, furan-2-carboxaldehyde **1c**, thiophene-2-carboxaldehyde **1d**, benzaldehyde **1e**, salicylaldehyde **1f**, 3-phenylpropanal **1g**, hexanal **1h**, 2-methylpentanal **1i**, and eicosanal **1j**, respectively, with hydroxylamine in the presence of $AgNO_3$ and vitamin $K_3$, affording adducts **2b–j** (Scheme 4).

In all cases, the products were obtained in excellent yields ranging from 81 to 92% (Table 3).

As observed from the aforementioned results, this procedure provides an interesting solution for the synthesis of hydroxamic acids from aldehydes. Advantages of this method include the preparation of hydroxamic acids in one step, the low-cost reaction setup, short reaction times, tolerance to ambient conditions, use of a clean photocatalytic reaction under visible light irradiation, and the obtainment of products in excellent yields without recourse to protection/deprotection strategies.
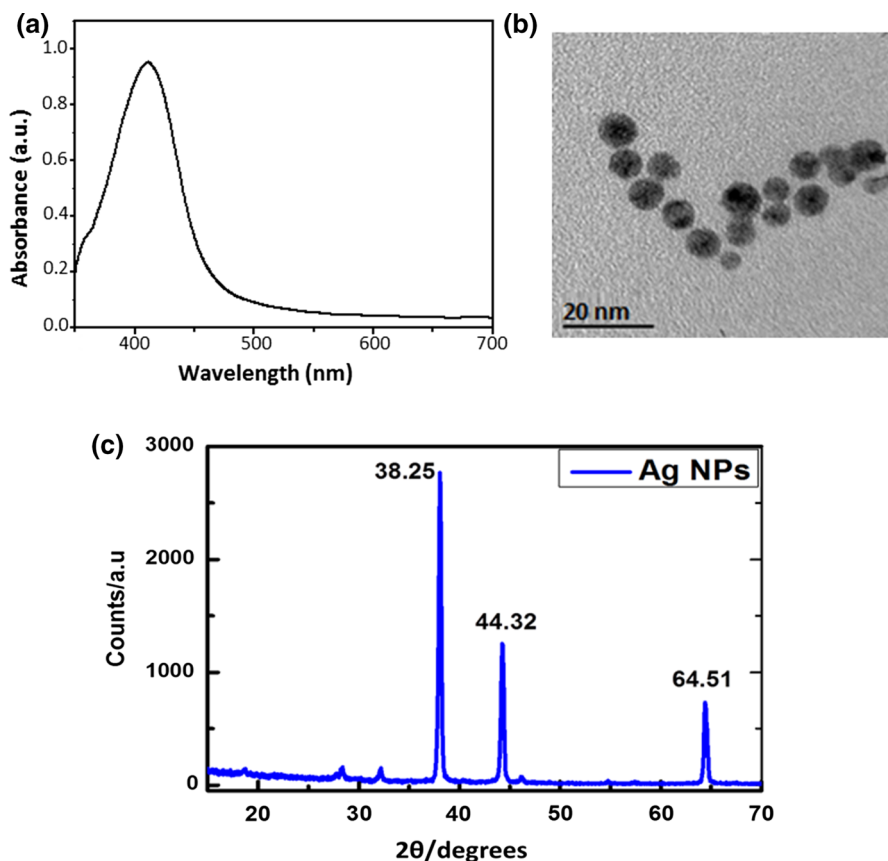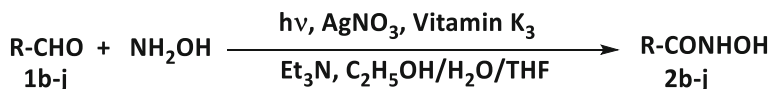
**(a)**

**(b)**

**(c)**

Fig. 4  **a** Absorption spectrum of the supernatant solution after completion of the reaction that indicates the formation of Ag NPs, **b** TEM image of the formed Ag NPs and **c** XRD pattern of the formed Ag NPs
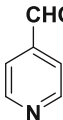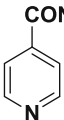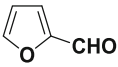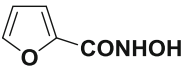
$$\text{R-CHO} + \text{NH}_2\text{OH} \xrightarrow[\text{Et}_3\text{N, C}_2\text{H}_5\text{OH/H}_2\text{O/THF}]{h\nu, \text{AgNO}_3, \text{Vitamin K}_3} \text{R-CONHOH}$$
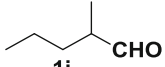
R-CHO + NH₂OH → R-CONHOH
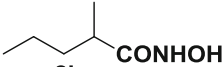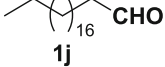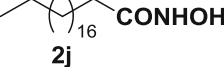1b-j                    2b-j
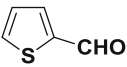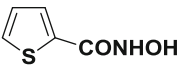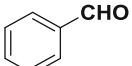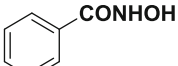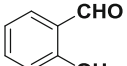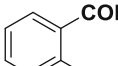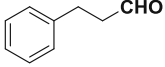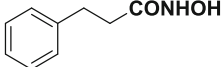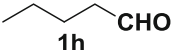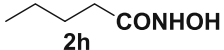
**Scheme 4**  The synthesis of a series of hydroxamic acids from aldehydes

## Conclusions

In summary, we have investigated a simple, efficient and green modified Angeli–Rimini procedure for the synthesis of heterocyclic, aromatic and aliphatic hydroxamic acids from aldehyde derivatives. The successful use of Ag nanoclusters in an unconventional reaction has been demonstrated. The mild reaction conditions employed, high product yields, short reaction times, and the absence of undesirable side products make this procedure more practical than previously reported methods. This approach should inspire novel applications of Ag nanocluster photocatalysts in organic synthesis.

**Table 3** Visible light-induced transformation of aldehydes **1b–j** to **2b–j**

| Substrate | Product | Yield % |
|---|---|---|
| CHO ![1b] **1b** | CONHOH ![2b] **2b** | 91 |
| CHO **1c** | CONHOH **2c** | 87 |
| CHO **1d** | CONHOH **2d** | 89 |
| CHO **1e** | CONHOH **2e** | 85 |
| CHO OH **1f** | CONHOH OH **2f** | 83 |
| CHO **1g** | CONHOH **2g** | 86 |
| CHO **1h** | CONHOH **2h** | 92 |
| CHO **1i** | CONHOH **2i** | 81 |
| CHO **1j** | CONHOH **2j** | 90 |

## Compliance with ethical standards

**Conflict of interest** The authors have declared no conflict of interest.

# References

1. A. Porcheddu, G. Giacomelli, J. Org. Chem. **71**, 7057 (2006)
2. K.S. Jain, K.A.A. Kumar, S.B. Bharate, R.A. Vishwakarm, Org. Biomol. Chem. **12**, 6465 (2014)
3. F.T. Wong, P.K. Patra, J. Seayad, Y. Zhang, J.Y. Ying, Org. Lett. **10**, 2333 (2008)
4. S.L. Yedage, B.M. Bhanage, Synthesis **47**, 526 (2015)
5. G.N. Papadopoulos, C.G. Kokotos, Chem. Eur. J. **22**, 6964 (2016)
6. J.C.S. Woo, E. Fenster, G.R. Dake, J. Org. Chem. **69**, 8984 (2004)
7. A. Gissot, A. Volonterio, M. Zanda, J. Org. Chem. **70**, 6925 (2005)
8. J.R. Martinelli, D.M.M. Freckmann, S.L. Buchwald, Org. Lett. **8**, 4843 (2006)
9. K. Thalluri, S.R. Manne, D. Dev, B. Mandal, J. Org. Chem. **79**, 3765 (2014)
10. B. Vasantha, H.P. Hemantha, V.V. Sureshbabu, Synthesis **2010**, 2990 (2010)
11. E.M. Muri, M.J. Nieto, R.D. Sindelar, J.S. Williamson, Curr. Med. Chem. **9**, 1631 (2002)
12. A. Yekkour, A. Meklat, C. Bijani, O. Toumatia, R. Errakhi, A. Lebrihi, F. Mathieu, A. Zitouni, N. Sabaou, Lett. Appl Microbiol. **60**, 589 (2015)
13. N. Türkel, J. Chem. Eng. Data **56**, 2337 (2011)
14. M. Harty, S.L. Bearne, J. Therm. Anal. Calorim. **123**, 2573 (2016)
15. H. Chen, C. Liu, M. Wang, C. Zhang, N. Luo, Y. Wang, H. Abroshan, G. Li, F. Wang, ACS Catal. **7**, 3632 (2017)
16. M. Miyauchi, H. Irie, M. Liu, X. Qiu, H. Yu, K. Sunada, K. Hashimoto, J. Phys. Chem. Lett. **7**, 75 (2016)
17. M.A. Koklioti, T. Skaltsas, Y. Sato, K. Suenaga, A. Stergiou, N. Tagmatarchis, Nanoscale **9**, 9685 (2017)
18. J.C. Ahern, S. Kanan, H.H. Patterson, Comments Inorg. Chem. **35**, 59 (2015)
19. H. Zhu, N. Goswami, Q. Yao, T. Chen, Y. Liu, Q. Xu, D. Chen, J. Lu, J. Xie, J. Mater. Chem. A **6**, 1102 (2018)
20. S. Abbet, A. Sanchez, U. Heiz, W.D. Schneider, A.M. Ferrari, G. Pacchioni, N. Rösch, J. Am. Chem. Soc. **122**, 3453 (2000)
21. Y. Liu, H. Tsunoyama, T.C. Akita, S. Xie, T.C. Tsukuda, ACS Catal. **1**, 2 (2011)
22. F.F. Schweinberger, M.J. Berr, M. Döblinger, C. Wolff, K.E. Sanwald, A.S. Crampton, C.J. Ridge, F. Jäcke, J. Feldmann, M. Tschurl, U. Heiz, J. Am. Chem. Soc. **135**, 13262 (2013)
23. U. Heiz, A. Sanchez, S. Abbet, W.D. Schneider, Chem. Phys. **262**, 189 (2000)
24. A.S. Wörz, K. Judai, S. Abbet, U. Heiz, J. Am. Chem. Soc. **125**, 7964 (2003)
25. Y. Attia, M. Samer, Renew. Sustain. Energy Rev. **79**, 878 (2017)
26. S. Yin, Z. Wang, E.R. Bernstein, Phys. Chem. Chem. Phys. **15**, 4699 (2013)
27. Y. Attia, D. Buceta, C. Blanco-Varela, M. Mohamed, G. Barone, M.A. López-Quintela, J. Am. Chem. Soc. **136**, 1182 (2014)
28. Y. Attia, D. Buceta, F. Requejo, L. Giovanetti, M.A. López-Quintela, Nanoscale **7**, 11273 (2015)
29. Y. Lu, W. Chen, Chem. Soc. Rev. **41**, 3594 (2012)
30. B. Adhikari, A. Banerjee, Chem. Mater. **22**, 4364 (2010)
31. N. Cathcart, P. Mistry, C. Makra, B. Pietrobon, N. Coombs, M. Jelokhani-Niaraki, V. Kitaev, Langmuir **25**, 5840 (2009)
32. S. Dai, X. Zhang, T. Li, Z. Du, H. Dang, Appl. Surf. Sci. **249**, 346 (2005)
33. W. Guo, J. Yuan, Q. Dong, E. Wang, J. Am. Chem. Soc. **132**, 932 (2010)
34. H.C. Yeh, J. Sharma, J.J. Han, J.S. Martinez, J.H. Werner, Nano Lett. **10**, 3106 (2010)
35. C.I. Richards, S. Choi, J.C. Hsiang, Y. Antoku, T. Vosch, A. Bongiorno, Y.L. Tzeng, R.M. Dickson, J. Am. Chem. Soc. **130**, 5038 (2008)
36. X.L. Guevel, B. Hötzer, G. Jung, K. Hollemeyer, V. Trouillet, M. Schneider, J. Phys. Chem. C **115**, 10955 (2011)
37. J. Xie, Y. Zheng, J.Y. Ying, J. Am. Chem. Soc. **131**, 888 (2009)
38. A. Mathew, P.R. Sajanlal, T. Pradeep, J. Mater. Chem. **21**, 11205 (2011)
39. N.K. Makhmudova, ZCh. Kadyrova, E.A. Del'yaridi, KhT Sharipov, Russ. J. Org. Chem. **37**, 866 (2001)
40. O. Kreye, S. Wald, M.A.R. Meier, Adv. Synth. Catal. **355**, 81 (2013)
41. G. Dettori, S. Gaspa, A. Porcheddu, L. De Luca, Adv. Synth. Catal. **356**, 2709 (2014)
42. A.R. Katritzky, N. Kirichenko, B.V. Rogovoy, Synthesis **2003**, 2777 (2003)
43. J. Schlupmann, F. Lendzian, M. Plato, K. Mobius, J. Chem. Soc. Faraday Trans. **89**, 2853 (1993)

44. N. Durán, P.D. Marcato, O.L. Alves, G.D. Souza, E. Esposito, J. Nanobiotech. **3**, 8 (2005)
45. A. Król-Gracz, P. Nowak, E. Michalak, A. Dyonizy, Acta Phys. Pol. A **121**, 196 (2012)
46. S.E. Selva, D. Martinez, M.J. Buceta, M.C. Rodriguez-Vazquez, M.A. Blanco, G.Egea Lopez-Quintela, J. Am. Chem. Soc. **132**, 6947 (2010)
47. K. Jyoti, M. Baunthiyal, A. Singh, J. Radiat. Res. Appl. Sci. **9**, 217 (2016)